HOSTED BY
ELSEVIER
Available online at www.sciencedirect.com
ScienceDirect
Soils and Foundations 60 (2020) 425–438
SOILS AND FOUNDATIONS
www.elsevier.com/locate/sandf

Technical Paper

# Influence of lining permeability and temperature on long-term behavior of segmented tunnel

Wei Li [a,*], Alireza Afshani [a], Hirokazu Akagi [a], Shigeaki Oka [b]

[a] Department of Civil Engineering, Waseda University, 3-4-1, Okubo, Shinjuku-ku, Tokyo 169-8555, Japan
[b] Tokyo Electric Power Company Holdings, Incorporated, 1-1-3, Uchisaiwai-cho, Chiyoda-ku, Tokyo 100-8560, Japan

Received 6 March 2019; received in revised form 17 January 2020; accepted 7 March 2020
Available online 17 April 2020

**Abstract**

The initial infiltration of ground water into tunnels excavated in soft clayey soils triggers the consolidation of the surrounding soil and imposes an extra load on the linings. This extra load may open the joints between rings and segments or intensify the deterioration of the joints. Relative soil-lining permeability, an important factor in the long-term behavior of tunnels, mainly depends on the condition and amount of joint opening between rings and segments. This study proposes a method for determining lining permeability based on the joint opening between rings only. The lining permeability value can be implemented and updated in coupled soil-water analyses during the entire consolidation process. In the final stages of consolidation, the values of the pore water pressure and water leakage reach a steady-state condition and the effect of seasonal temperature changes inside the tunnel becomes important. Furthermore, determination of the lining permeability under the influence of the temperature inside the tunnel is attempted. Long-term measured field data of an aged tunnel along with a coupled soil-water model are employed to verify and explain the long-term behavior of segmented tunnels using the proposed method. In addition, the applicability and limitations of the proposed method are presented and discussed.


*Keywords:* Long-term behavior; Lining permeability; Tunnel settlement; Water leakage; Joint deterioration; Coupled soil-water finite element method

## 1. Introduction

In clayey soil, the long-term post-construction behavior of segmented tunnels is usually accompanied with continuous ground surface settlement. This is commonly induced by the consolidation of soft soil around the tunnels because of water leakage into the tunnels.

Through tunnel deterioration, underground water finds a way to infiltrate tunnels, and the tunnel acts as a drainage boundary due to the increase in the lining permeability (Mair, 2008; Nyren, 1998; Harris, 2002; Ward, 1981). Water leakage into the tunnel reduces the pore pressure and increases the effective stress in soils around the tunnel (Shirlaw, 1995). This leads to extra loads on the lining and intensifies the opening of joints and cracks. The increase in joint and crack opening accelerates water leakage into the tunnel. This repeated chain of events causes large lining deformation and considerable water inflow into the tunnel (No, & International Tunnelling Association, 2000; Shen et al., 2014; Soga, Laver, & Li, 2017).

The long-term behavior of tunnels has been studied by several researchers. Mair and Taylor (1997) showed that the relative soil-lining permeability is a major factor that influences the development of post-construction settlement. The value of the relative permeability can change the drainage condition around the tunnel and also affect the shape of the ground surface trough. For instance, it was demonstrated that in the case of high relative permeability,

Peer review under responsibility of The Japanese Geotechnical Society.
* Corresponding author.
*E-mail address:* wei@fuji.waseda.jp (W. Li).

https://doi.org/10.1016/j.sandf.2020.03.005

post-construction settlement troughs are significantly wider than short-term troughs associated with tunnel construction.

Gourvenec et al. (2005) carried out a field study of ground conditions around an old tunnel in London clay and found that the tunnel lining is nearly impermeable. This was attributed to the high observed pore water pressure in the surrounding clay with high permeability around the tunnel.

Mair (2008) summarized many previous studies on field measurements of long-term settlements and demonstrated that the magnitude of long-term ground movements and tunnel lining distortion depends on the relative soil-lining permeability along with other factors. He also reported the results of two-dimensional finite element analysis of the influence of soil permeability anisotropy and drainage conditions of the tunnel lining on long-term surface settlement. The results showed that the magnitude of long-term settlement and troughs in the case of anisotropic soils is larger than that in the case of isotropic soils.

Wu et al. (2011) and Zhang et al. (2013) conducted coupled soil-water finite element analysis and established a linear relationship between ground settlement and water discharge into the tunnel. However, one of the challenges in these studies was the determination of the amount of water discharge into the tunnel in soft clay (Soga, Laver, & Li, 2017).

As it is difficult to quantify the permeability of the tunnel lining, Wongsaroj et al. (2011, 2013) proposed a method to relate the relative soil-lining permeability to the dimensionless surface settlement in order to predict the long-term surface settlement by using a simplified one-dimensional flow model. The results of finite element analysis were compared with field-measured settlements induced by a single open-face tunnel construction in heavily over-consolidated London clay. Finally, a relationship was established for predicting the long-term consolidation settlement induced by the open-face tunneling cases of the Jubilee Line westbound tunnel and the Heathrow Express trial tunnel.

Li et al. (2015) carried out a series of three-dimensional coupled soil-water finite element analyses to investigate the long-term behavior of an old cast-iron cross passage tunnel in stiff London clay. The short- and long-term effects of relative permeability on ground response and tunnel lining behavior were examined against field observations.

On the basis of these studies, Laver et al. (2016) extended the work of Wongsaroj et al. (2013) and proposed a new method to estimate both vertical and horizontal settlement induced by consolidation. A new relative soil-lining permeability index was proposed using a more realistic radial flow model. The proposed method was verified considering the case studies conducted by Wongsaroj et al. (2013) in London clay. They also demonstrated the validity of using the proposed method to evaluate long-term surface settlement if a database of lining permeability values for different lining types.

On the other hand, Shin et al. (2012) focused on lining permeability by considering only the joints between segments in a two-dimensional model and found that the mechanical and hydraulic behavior of segmented tunnels can be represented by a combined model of a beam and solid elements. They also investigated the relative joint-lining permeability. It was concluded that even a small increase in the opening of joints results in a significant increase in water leakage, and in the design phase, long-term leakage due to joint deterioration can be simply estimated by the lining deformation.

Few studies have investigated the lining permeability due to the opening of joints between rings. Moreover, in most previous studies, lining permeability has been considered a constant parameter along the tunnel and also during the consolidation process (Soga, Laver, & Li, 2017). By deformation of the tunnel lining in the longitudinal direction under consolidation load, ring joints play a key role in the lining permeability. This paper proposes a method to determine the lining permeability based on the opening of joints between rings. The proposed method can be employed in the numerical investigation of any consolidation analysis. The opening of joints is calculated on the basis of the deformed shape of the lining at each desired step of consolidation. Further, different values of the soil-lining permeability ratio from fully impermeable to fully permeable tunnel lining and leakage from the top or the bottom of the lining can be simulated using this method.

In the final stages of consolidation, the consolidation-induced water leakage is small or nearly non-existent. At this time, the effect of seasonal changes in temperature inside the tunnel becomes important. The amount of water leakage and lining permeability are affected by temperature changes inside the tunnel as well as expansion or shrinkage of the concrete volume. In addition, a relationship between the temperature inside the tunnel and the lining permeability is established.

## 2. Introduction of an old segmented tunnel

To investigate the influence of lining permeability and temperature on the long-term tunnel lining behavior, a case of an aged segmented tunnel is introduced in this study. The tunnel was built in Japan with an overburden depth range of 8.5–14.0 m along its path in soft clayey soil. It has a total length of 2217 m and is used as an electrical transmission tunnel. Five ventilating shafts (VS) were constructed along the tunnel for ventilation and easy access into the tunnel. The first phase of construction between VS No.1 and VS No.3 (with a length of 1028 m) was completed in 1980 and the second phase between VS No.3 and VS No.5 (with a length of 1189 m) was completed in 1981.

In recent years, increased water leakage due to the deterioration of lining has been reported in the part of the tunnel between VS No.4 and VS No.5 with a total of 696 rings; therefore, our study focuses on this part. Fig. 1 shows the plan view of the site. The railway shown in Fig. 1 lies on the

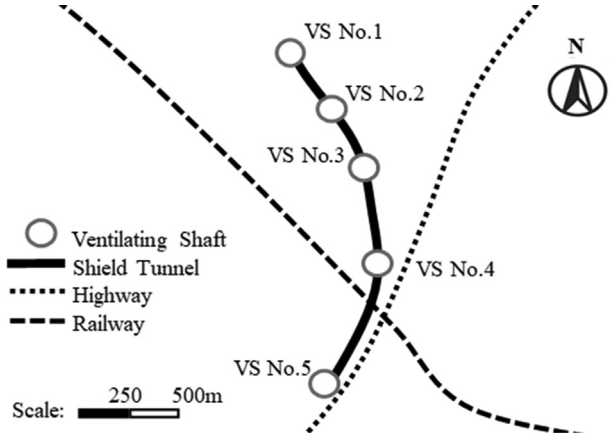


Fig. 1. Plan view of the site.

top of an embankment, and was built 10 years before tunnel construction.

### 2.1. Structural details of the tunnel

Each of the tunnel rings includes 6 reinforced concrete segments (with a width of 0.9 m and a thickness of 0.25 m) with a flat bar (FB) inside, and has an outer and inner diameter of 4.0 m and 3.5 m, respectively, as shown in Fig. 2(a) and (b). Fig. 2(c) and (d) show the segment joints in the longitudinal direction and ring joints in the circumferential direction, respectively, and both are interconnected by steel bolts and sealing rubber. The design Young's modulus of the segmented concrete is 32.0 MPa.

### 2.2. Long-term behavior of the tunnel

Ten years before tunnel construction in 1971, an embankment was constructed close to VS No. 4 beneath the railway line. It was found that during these 10 years, the soils beneath the embankment consolidated under the embankment load.

In 1996, an abnormality was discovered in the tunnel during periodic maintenance. At that time, 77 bolts from the steel shelf of cables were broken, a maximum vertical deformation of 12.4 mm inside the tunnel was recorded (see Fig. 2(b)), and a number of cracks were observed. Fig. 3(a) shows the location of a broken bolt from the steel shelf of cables and Fig. 3(b) shows the location of cracks at the crown of the segments. In 2005, the number of broken bolts was increased to 346 and the maximum measured vertical deformation reached 17.2 mm.

The displacement at the invert along the longitudinal direction of the tunnel was measured from the invert of the first ring in 2001 and 2010. The difference in displacement between 2001 and 2010 is shown in Fig. 4(a). Fig. 4(b). As can be seen in Fig. 4, the small settlement beneath the embankment is comparable with the large settlement at the location of R444 with a value of 11.8 mm and that at the location of R600 with a value of 11.9 mm. This implies that the tunnel section outside the zone under the embankment has experienced a progressive consolidation load.

In 2005, 2011, and 2013, the locations of water leakage and cracks were inspected by ring number. Field observations showed that leakage occurred at locations near the ring joints. The sealing rubber used for waterproofing between the joints was an extremely old non-vulcanized rubber made in the 1980s (Ariizumi et al., 2006; Tunnel Library 23, 2010). Because there was little information about the sealing rubber itself, its effect was unclear.

Fig. 5 shows the area of wet patches due to water leakage into the tunnel by rings between VS No.4 and VS. No.5. Small amounts of the wet patch area under the embankment (R1 to R270) are noticeable as well as large ones in the zone outside the embankment (R271 to R696). The data shown in Figs. 4(b) and 5 indicate that considerable leakage and displacement of the tunnel invert have occurred in the rings outside the influence zone of the embankment under the consolidation load.

To investigate the hydraulic behavior of the tunnel lining and surrounding ground, the pore water pressure was monitored from 2008 to 2010. The pore water pressure was measured by pore pressure gauges at a point located 3.0 m away from the tunnel. The gauges were installed through the existing holes for backfill grouting near the invert of the tunnel (see the left graph in Fig. 6). Fig. 6 shows the measured pore water pressure at the sections near R295 and R537. The pore water pressure value at R295 decreased from 125.6 kPa to 97.5 kPa; however,

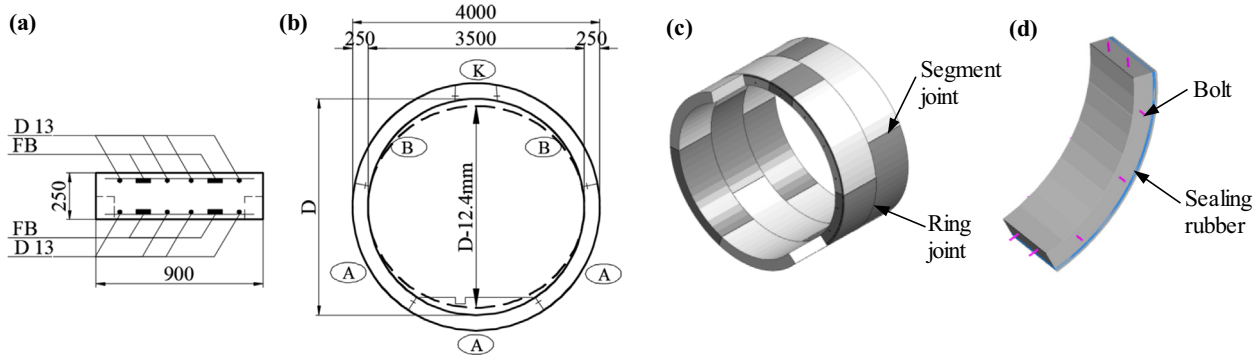


Fig. 2. Structural details of the tunnel.

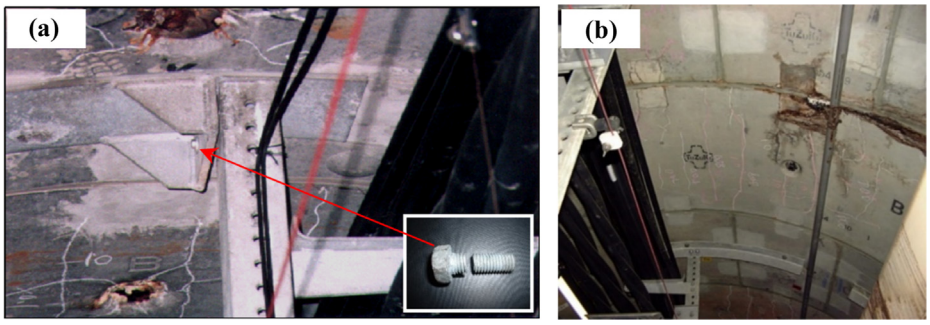


Fig. 3. (a) Broken bolts at steel cable shelf; (b) cracks at the crown of the segment.

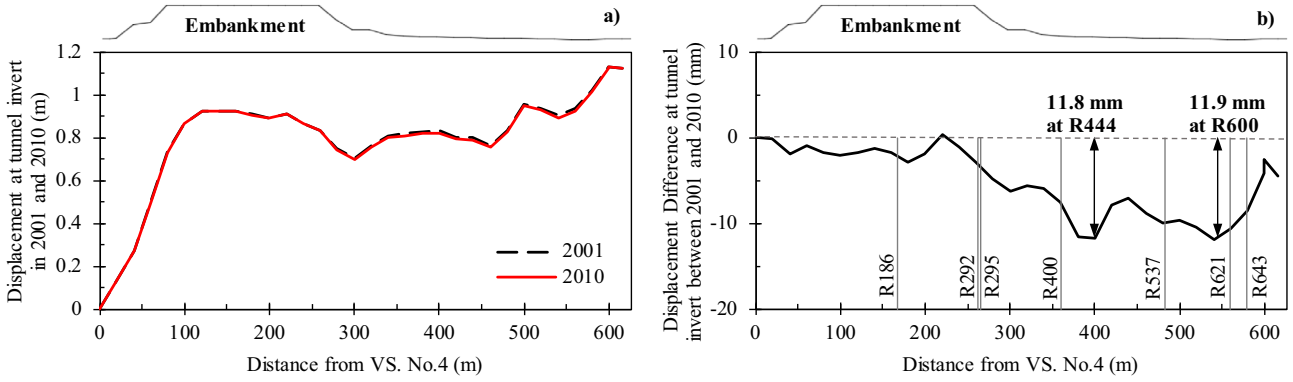


Fig. 4. Displacement difference at tunnel invert between 2001 and 2010.

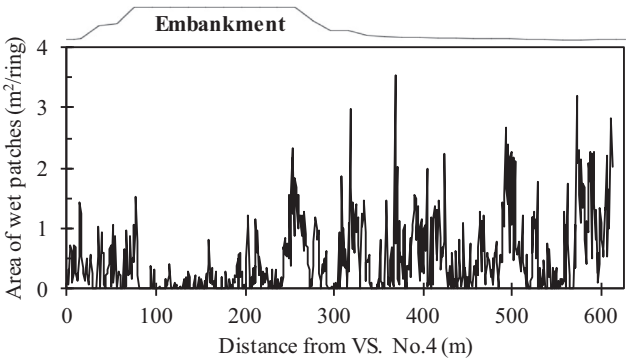


Fig. 5. Area of wet patches by the ring number.

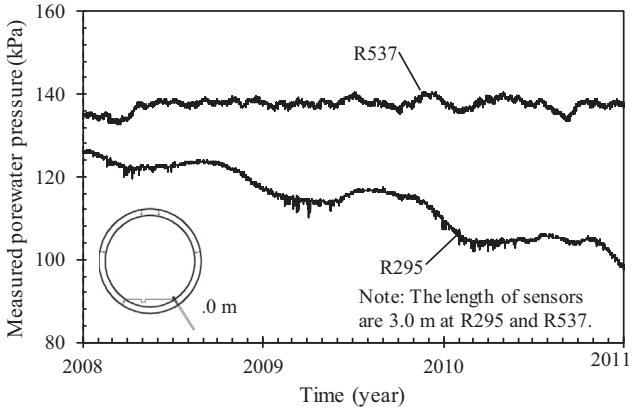


Fig. 6. Measured pore water pressure by time.

the value at R537 was nearly unchanged (137 kPa). Both pore pressure measurements are outside the zone of the embankment influence.

## 3. Lining permeability

Field observations show that segments of concrete lining can be considered to be practically impermeable owing to the low permeability of well-cured concrete, and water leakage commonly occurs through ring joints. Accurate estimation of the lining permeability based on the permeability of the lining segments and joints is difficult (Murillo et al., 2014; Shin et al., 2012; Wongsaroj et al., 2013) and requires extensive field measurements. In this study, investigation of the lining permeability was attempted on the basis of the permeability of jointed rocks. The original equation used for the permeability of jointed rocks is taken, and it is applied to the lining permeability with modifications.

### 3.1. Permeability of jointed rock

The flow of water through rock fissures has been extensively studied by Huitt (1956), Snow (1968), Louis (1969), Sharp (1970), Maini (1972), and others by following the same method used by Wyllie and Mah (2014). To obtain

the permeability of jointed rock, Davis (1969) simplified the problem to that of the determination of the equivalent permeability of a planar array of parallel smooth cracks as follows:

$$k = \frac{g \cdot e^3}{12v \cdot b} \tag{1}$$

where $k$ is equivalent permeability (m/s), $e$ is the opening of cracks or fissures (m), $g$ is the gravitational acceleration (=9.81 m/s$^2$), $b$ is the spacing between cracks or fissures (m), and $v$ is the coefficient of kinematic viscosity (=1.01 × 10$^{-6}$ m$^2$/s for pure water at 20 °C).

### 3.2. Permeability of tunnel lining

Shin et al. (2012) and Murillo et al. (2014) used Eq. (1) to evaluate the leakage at segment joints of tunnels and the permeability of tunnel drainage systems. In long-term deformation of tunnels, considerable opening develops between rings in the longitudinal direction; therefore, only the joint opening between rings is considered in this study. Fig. 7(a), (b), (c), and (d) show the schematics of a jointed segment, closed ring joint, ring joint opening from the bottom, and ring joint opening from the top, respectively. The spacing between cracks (i.e., parameter b in Eq. (1)) is defined as the distance between ring joints that is equal to the width of the segment. It is assumed that the surface of the ring joint opening is smooth, and the effect of the sealing rubber is not considered. In addition, the maximum joint opening can occur at the bottom or the top of the lining based on the deformed shape of the tunnel under the consolidation load in the longitudinal direction. The maximum opening is assumed to change linearly to zero at the top or bottom, as shown in Fig. 7 – (c) and (d), respectively. Based on these assumptions, the lining permeability is expressed by considering the ring joints as follows:

$$k_t = \frac{g \cdot {w_a}^3}{12v \cdot s} = \alpha \cdot \frac{g \cdot w^3}{12v \cdot s} \tag{2}$$

Assuming the ring joint opens linearly from the bottom (see Fig. 7 – (c)), in this case, the opening is 0 at the top and maximum value $w_{max}$ at the bottom. Hence, the average opening $w_a$ is equal to $\frac{w_{max}}{2}$. If the gauge is installed with an angle $\beta$ from the bottom and the measured value of opening is $w$, the relationship between $w_{max}$ and $w$ is $\frac{w_{max}}{\pi} = \frac{w}{(\pi-\beta)}$. Thus, $w_a = \frac{w_{max}}{2} = \frac{\pi}{2(\pi-\beta)} w$. Substituting this equation into Eq. (2), the permeability $k_t = \frac{g \cdot {w_a}^3}{12v \cdot s} = \frac{g}{12v \cdot s} \cdot \left[\frac{\pi}{2(\pi-\beta)} w\right]^3 = \left[\frac{\pi}{2(\pi-\beta)}\right]^3 \cdot \frac{g \cdot w^3}{12v \cdot s}$. Defining $\alpha$ as an angle multiplier, the value of $\alpha$ is

$$\alpha = \left[\frac{\pi}{2(\pi - \beta)}\right]^3 \tag{3}$$

where $w_a$ is the average opening of the ring joint (m), $w_{max}$ is the maximum opening at the bottom or top of the ring joint (m), $w$ is the gauge opening of the ring joint (m), $\beta$ is the angle of the gauge location from the maximum opening in radians, $\alpha$ is the angle multiplier, $g$ is the gravitational acceleration (=9.81 m/s$^2$), $s$ is the spacing between the ring joints (m), and $v$ is the coefficient of kinematic viscosity (=1.01 × 10$^{-6}$ m$^2$/s for pure water at 20 °C).

## 4. Effect of temperature

Here, the effect of temperature on the lining permeability is studied. In 2002, the opening of the ring joint and the temperature inside the tunnel were monitored by the installation of two crack displacement transducers with an accuracy of 0.01 mm (DC2-5 and DC2-6), shown in the upper left picture in Fig. 9, and four digital thermometers (A2, B2, C2, and D2), respectively.

Fig. 8 shows the changes in the measured ring joint opening and temperature inside the tunnel by month in 2002. The temperature variation is divided into two distinct patterns of cold and hot seasons with temperatures ranging between 27.5 and 32.0 °C and 32.7–37.4 °C, respectively. Field measurements show that owing to the effect of the tunnel temperature on the volumetric change of the concrete lining, the opening of joints widens and shrinks in hot and cold seasons, respectively, and this behaviour is repeated annually.

The volume of water discharged into the tunnel varies according to the changes in the values of the joint opening. The total volume of water discharge is calculated by measureing the approximately surface area and the depth of water collected. Fig. 9 shows the total volume of water discharged between VS No. 4 and VS No. 5 from June 2017 to May 2018. In the cold months of the year (Nov. to Mar.),

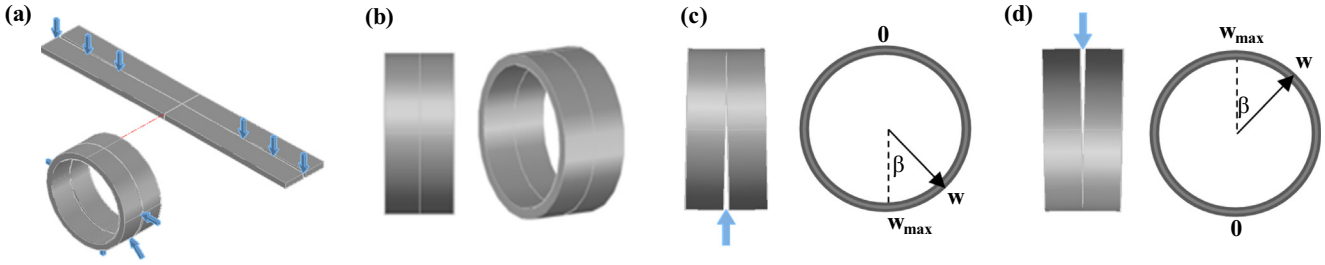


Fig. 7. (a) Jointed tunnel segment; (b) Closed ring joint; (c) Ring joint opening from the bottom; (d) Ring joint opening from the top.

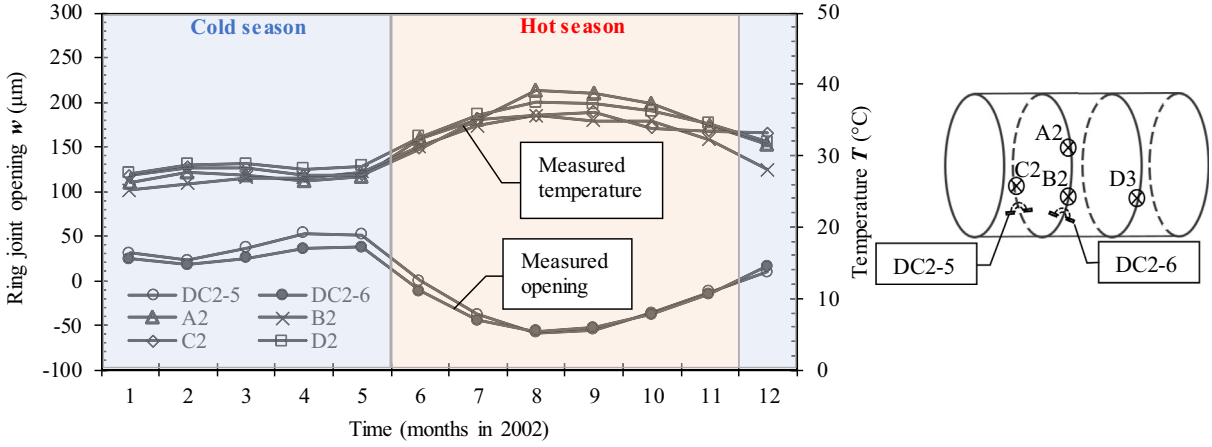


Fig. 8. Changes in the ring joint opening and temperature inside tunnel over time.

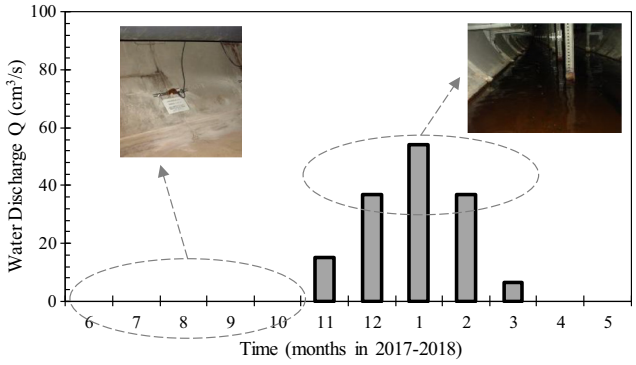


Fig. 9. Monthly total water discharge in 2017 and 2018.

there was considerable water flow into the tunnel, while no water leakage was recorded in the other months.

Oka et al. (2017) studied part of the measurement data of the tunnel in this study and proposed a relationship between the gauge opening ($w$) and the tunnel temperature ($T$) in the form of Eq. (4) and Fig. 10(a). Fig. 10(a) shows that the gauge opens with a decrease in temperature and closes with an increase in temperature. These relationships were obtained using only the temperature-joint opening data of sensor D2 from limited months taken in 2002. In this study, by using the entire range of the measured data and sensors A2, B2, C2, and D2, Fig. 10(b) and Eq. (5) are proposed for better correlation between the gauge opening and the tunnel temperature in cold and hot seasons. These data are also shown in Fig. 8. It can be seen that while the opening changes slightly in cold season, it changes significantly in the hotter seasons. Similar behavior is shown in Fig. 10 – (b), where the slope of the predicted curve in the hot season (red zone) is steeper than that in the cold season (blue zone). Note that the slopes of the two curves are predicted to change at approximate 31 ℃.

$$w = \begin{cases} -13.0T + 370.7(Tdecrease) \\ -12.3T + 428.0(Tincrease) \end{cases} \quad (4)$$

$$w = \begin{cases} -4.72T + 162.76(coldseason) \\ -9.68T + 308.76(hotseason) \end{cases} \quad (5)$$

By substituting Eq. (5) into Eq. (2), a relationship between the lining permeability ($k_t$) and the temperature inside the tunnel ($T$) is proposed as Eq. (6). This equation is suggested for use for the range of $5 \times 10^{-12} m/s \leq k_t \leq 5 \times 10^{-8} m/s$ for the tunnel in this study. The explanation for the selection of this range is given in section 5.3 (2).

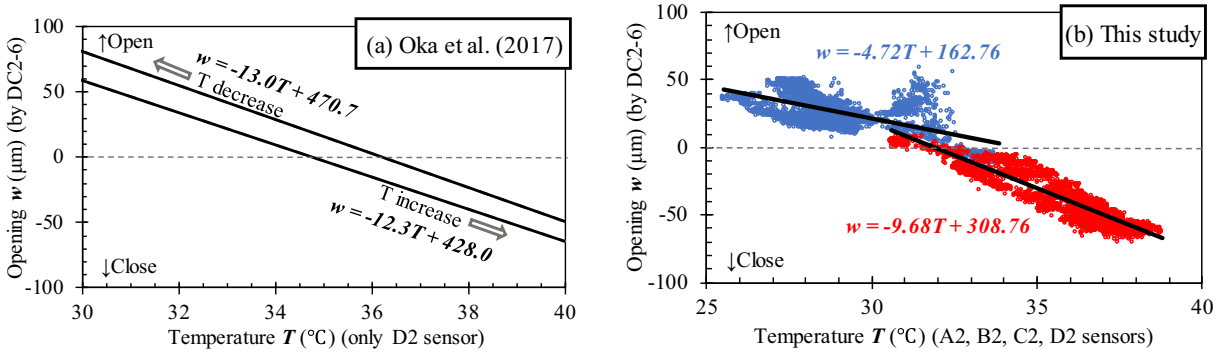


Fig. 10. Changes in ring joint opening by temperature: (a) Oka et al. (2017); (b) This study.

$$k_t = \begin{cases} \alpha \cdot \frac{g(-4.72T+162.76)^3}{12vs}(coldseason) \\ \alpha \cdot \frac{g(-9.68T+308.76)^3}{12vs}(hotseason) \end{cases} 5 \times 10^{-12} m/s \le k_t \le 5 \times 10^{-8} m/s \quad (6)$$

## 5. Numerical model

### 5.1. Material parameters

The proposed equations for the permeability of the joint opening and temperature-dependent lining permeability are employed in a three-dimensional coupled soil-water modeling of consolidation in cohesive soil around an aged tunnel in Japan. The numerical model is used to study the mechanical and hydraulic behavior of the concrete lining and surrounding soils. Fig. 11 shows the part of the longitudinal section of the soil profile and tunnel used for numerical modeling in this study, between VS. No.4 and VS. No.5.

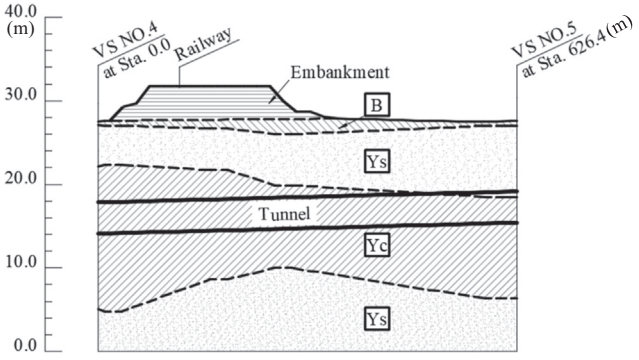


Fig. 11. Longitudinal profile of soil layers and tunnel.

The borehole data, the results of laboratory and in-situ tests are used to determine the orientation and parameters of the soil layers. The embankment was constructed on the backfill layer (B). Beneath the backfill, the soils are mainly composed of alluvial sand (Ys). The tunnel was built in the alluvial clayey soil layer known as Yurakucho clay (Yc) in Japan. The thickness of the Yc layer is approximately 9.9–17.5 m, which has been reported to have a standard penetration test value ($N_{SPT}$) near zero. The Ys layer at the bottom is mainly composed of sand and is known as the No. 7 layer in Japan. The layers beneath the Ys layer are composed of gravel and their $N_{SPT}$ values are larger than 50; they are therefore not included in the numerical model. Table 1 lists the parameters used for the soil layers in the model. The model of modified Cam-clay (Ports and Zdravkovic, 2001) is employed to present the behavior of the Yc layer, and a linear elastic model is used for the other soil layers and concrete material.

The actual joints between segments and rings have not been modeled in this study. The segmented tunnel is considered as a continuous lining with reduced rigidity by applying reduction factor $\eta$ to the bending rigidity ($EI$) of the tunnel as follows (Tunnel Library 23, 2010):

Table 1
List of soil parameters used in the numerical model.

| Soil properties | Symbol | | Embankment & backfill (B) | Alluvial sand (Ys) | Yurakucho clay (Yc) | Sand (Ys) | Test method or used equation |
|---|---|---|---|---|---|---|---|
| Analysis model | | | Elastic | Elastic | Modified Cam-clay | Elastic | |
| Unit weight | $\gamma$ | kN/m$^3$ | 17.5 | 17.5 | 16.4 | 17.5 | Physical test |
| Young's modulus | $E$ | kN/m$^2$ | 9300 | 4000 | 4000 | 4000 | Triaxial CD test |
| Effective Poisson's ratio | $v'$ | — | 0.33 | 0.33 | 0.317 | 0.33 | Consolidation test for Yc, common values for other layers |
| Permeability coefficient In-situ permeabilitytest by boreholes | $k$ | m/sec | $4.11 \times 10^{-9}$ | $4.24 \times 10^{-5}$ | $4.11 \times 10^{-9}$ | | $5.9 \times 10^{-6}$ |
| Void ratio | $e_0$ | — | 1.105 | 1.105 | 1.353 | 1.105 | $e = (\gamma_w G_s - \gamma_{sat})/(\gamma_{sat} - \gamma_w)$ |
| Coefficient of earth pressure | $K_0$ | — | 0.5 | 0.5 | 0.464 | 0.5 | $K$-Consolidation test for Yc, common values for other layers |
| Gradient of isotropic normal consolidation line | $\lambda$ | — | — | — | 0.233 | — | Consolidation test (=0.434$C_c$) |
| Gradient of isotropic swelling line | $\kappa$ | — | — | — | 0.018 | — | Consolidation test (=0.434$C_s$) |
| Slope of critical state line | $M$ | — | — | — | 1.41 | — | $M = 6\sin\varphi'/(3-\sin\varphi')$ |
| Dilatancy coefficient | $D$ | — | — | — | 0.065 | — | $D = \lambda\Lambda/(M + M\,e_0)$ $\Lambda = 1-\kappa/\lambda = 1-Cs/Cc$ |
| Permeability changing ratio | $C_k$ | — | — | — | 0.6765 | — | $C_k = e_0/2$ |

*Notes:* $\gamma_{sat}$ is the saturated unit weight of soil, $G_s$ is the specific gravity, $C_c$ is the compression index, $C_s$ is the swelling index, $\varphi'$ is the effective-stress friction angle, $\lambda$ is the gradient of isotropic normal consolidation lines (=0.434$C_c$), $\kappa$ is the gradient of isotropic swelling lines (=0.434$C_s$).

$$(EI)_{eq} = \eta \cdot (EI) = \frac{cos^3 \varnothing}{cos\varnothing + (\frac{\pi}{2} + \varnothing) \cdot sin\varnothing} \cdot (EI) \quad (7)$$

where $(EI)_{eq}$ is the equivalent bending stiffness of the ring, $(EI)$ is the bending stiffness of the segment, $\varnothing$ is the angle from the spring-line to the neutral axis of the section under the bending moment, and $\eta$ is the reduction factor.

### 5.2. Analysis stages

Table 2 shows the time-dependent stages of the analyses. Two initial steps are used to create the initial stress and hydraulic condition in the model. The embankment was constructed over two months in 1971 and the soils beneath it were allowed to consolidate for ten years from 1971 to 1981. Then, the tunnel was excavated over two months in 1981 and the tunnel-induced consolidation occurred during 29 years from 1981 to 2010.

### 5.3. Determination of lining permeability

(1) Water flow conditions

According to Fig. 5, the area of wet patches owing to water flow into the tunnel is small in the range of R1 to R270. This range is considered to be the no-water flow range. Moreover, based on the field observations, wet patches in the range of R666 to R696 are believed to have been created because of water from the ventilating shaft and not from the lining. This range is also taken as the no-water flow range. The range of R271 to R665 is considered as the water flow range in the analyses.

Table 2
Analysis stages.

| Stage | Period |
|---|---|
| Initial-stress | — |
| Initial-seepage | — |
| Embankment construction | 1971 |
| Embankment consolidation | 1971–1981 |
| Tunnel construction | 1981 |
| Tunnel consolidation | 1981–2010 |

(2) Upper and lower bound of lining permeability

Laver et al. (2016) proposed a new relationship between relative soil-lining permeability $RP$ and the dimensionless surface settlement $DS$, which is given respectively by Eq. (8) and Eq. (9).

$$RP = \frac{DK_t\gamma_w}{2k_s} ln\left(\frac{2C_{clay}}{D} + 1\right) \quad (8)$$

where $K_t$ is the lining seepage coefficient ($= k_t/\gamma_w t$), $k_t$ is the lining permeability, $t$ is the lining thickness, $k_s$ is the average equivalent soil permeability ($= \sqrt{k_h k_v}$), $k_h$ is the soil permeability in the horizontal direction, $k_v$ is the soil permeability in the vertical direction, $C_{clay}$ is the cover thickness of clay above the tunnel crown, and $D$ is the lining diameter.

$$DS = \frac{NS_{cmax(ss)} - NS_{cmax(ssi)}}{NS_{cmax(ssp)} - NS_{cmax(ssi)}} \quad (9)$$

where $NS_{cmax(ss)}$ is the non-dimensional long-term settlement in the steady-state condition, $NS_{cmax(ssi)}$ is for the fully impermeable lining case, and $NS_{cmax(ssp)}$ is for the fully permeable lining case.

Laver et al. (2016) suggested that the tunnel is fully impermeable if $RP < 0.01$, and it is fully permeable if $RP > 100$. In this study, the relation between $RP$ and $DS$ was obtained numerically. Fig. 12(a) shows the $RP$-$DS$ graph for sections of R186, R292, R400, and R643. To develop the $RP$-$DS$ for each section, the lining permeability ($k_t$) was changed from $1.0 \times 10^{-13}$ to $1.0 \times 10^{-6}$ m/s and the ground surface settlement above each section for the corresponding $k_t$ was obtained. Fig. 12(b) shows DS versus lining permeability, which was obtained from Fig. 12(a). The relationship shown in Fig. 12(b) is used to determine the upper and lower bounds of the lining permeability. By doing so, the range of $5.0 \times 10^{-8}$ to $5.0 \times 10^{-8}$ m/s was determined. For the cases of $k_t < 5.0 \times 10^{-8}$ m/s and $k_t > 5.0 \times 10^{-8}$ m/s, the lining is considered to be fully impermeable and fully permeable, respectively.

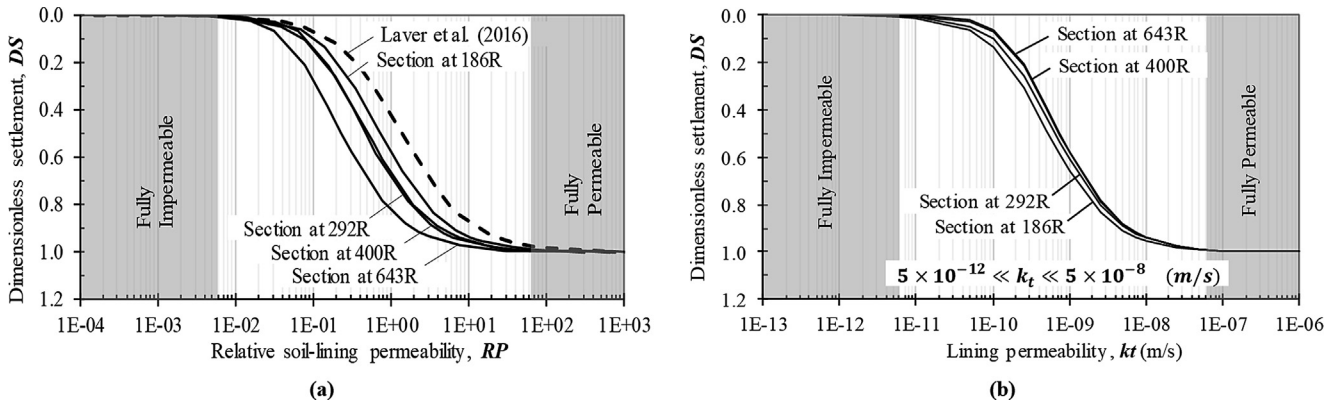


Fig. 12. (a) $DS$–$RP$ graph; (b) $DS$-$kt$ graph.

(3) Lining permeability from 1981 to 2002

It can be assumed that the tunnel lining is fully impermeable at the time of construction completion in 1981; thus, the value of $5.0 \times 10^{-12}$ m/s is assigned to all the rings as an initial value of the lining permeability. The $k_t$ value in 2002 is calculated using the ring joint opening data of gauge DC2-5 and DC2-6, and Eqs. (2) and (3). Table 3 lists the calculated values of the required items. From Table 3, $k_t = 4.69 \times 10^{-9}$ m/s is determined to be used in 2002 for the range of R271 to R665.

From 1981 to 2002, there was no water leakage or joint opening measured data, and under a simplifying assumption, the lining permeability $kt$ is assumed to change linearly between the initial value in 1981 and the calculated value in 2002. Fig. 13 shows the logarithmic values of $kt$ by time used in the numerical analysis from 1981 to 2002.

(4) Lining permeability from 2002 to 2010

The values of the lining permeability after 2002 are determined by obtaining the joint opening per ring directly from the numerical results and substituting them into Eqs. (2) and (3). The method for calculating the ring joint opening from the numerical output is as follows:

Fig. 14 shows deformed rings of the segmented lining under the load. The rotation angle $\theta$ of the ring joint opening is the same as the rotation angle between the center line of two neighbor rings. The slope $k$ of the center lines of each ring is calculated using Eqs. (10) and (11). The coordinates of the deformed nodes are obtained from the numerical results at each analysis step during tunnel consolidation. From 2002 to 2010, the maximum opening at the tunnel invert or crown is calculated using Eq. (12).

$$k_i = \frac{Z_{i+1} - Z_i}{Y_{i+1} - Y_i} \tag{10}$$

$$\theta = atan\left(\frac{k_{i+1} - k_i}{1 + k_i \cdot k_{i+1}}\right) \tag{11}$$

$$w_{max} = \theta \times D \tag{12}$$

where $k_i$ is the slope of the line at the middle of each ring, $\theta$ is the rotation angle of the center lines between two neighbor rings, $Z_i$ and $Y_i$ are the Z and Y coordinates of the points on the lines at the middle of the ring, and $D$ is the outer diameter of the tunnel.

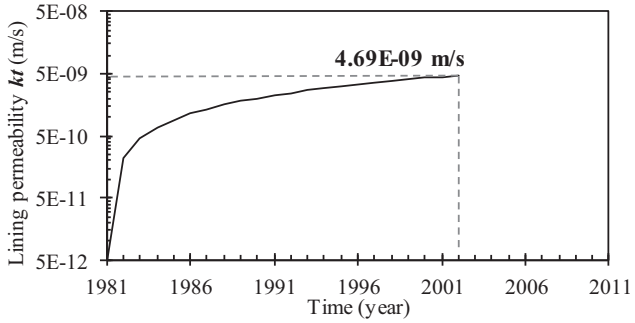


Fig. 13. Values of lining permeability by time used in the analysis from 1981 to 2002.

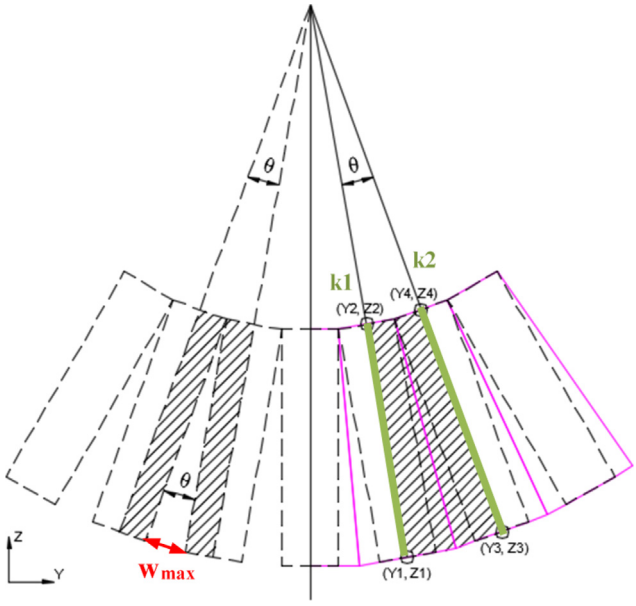


Fig. 14. Deformed rings of segmented lining and configuration of ring joint opening calculation.

(5) Summary

Table 4 summarizes the lining permeability values used in the numerical analyses.

Table 3
Calculation of lining permeability in 2002.

| Item | Symbol | Value | Unit |
|---|---|---|---|
| Measured value of initial ring joint opening from DC2-5 | $w_1$ | 32.0 | μm |
| Measured value of initial ring joint opening from DC2-6 | $w_2$ | 25.8 | μm |
| Average of measured values from DC2-5 and DC2-6 | $w$ | 28.9 | μm |
| Angle of gauge location from maximum opening (see Fig. 7c) | $\beta$ | 30 | Degree |
| Maximum opening of ring joint (at tunnel invert) | $w_{max}$ | 34.7 | μm |
| Average opening of ring joint (by using Eq. (3)) | $w_a$ | $1.73 \times 10^{-5}$ | m |
| Permeability of lining (by using Eq. (2)) | $k_t$ | $4.69 \times 10^{-9}$ | m/s |

*Notes:* $g$ is the gravitational acceleration (=9.81 m/s$^2$), $s$ is the spacing between the ring joint and is equal to the width of the segment (=0.9 m), and $v$ is the coefficient of kinematic viscosity (=$1.01 \times 10^{-6}$ m$^2$/s).

Table 4
Summary of determined $k_t$ values.

| Stage | Period | Lining permeability $k_t$ (m/s) | Note |
|---|---|---|---|
| Tunnel construction | 1981 | $5.0 \times 10^{-12}$ | Fully impermeable condition is applied. |
| Tunnel consolidation | 1981–2002 | $5.0 \times 10^{-12} \sim 4.69 \times 10^{-9}$ | It changes according to the value shown in Fig. 13. |
| Tunnel consolidation | 2002–2010 | Varies | It is obtained from numerical results of the deformed ring coordination and equations (2), (3), (10), (11), and (12). |

## 6. Verification

To evaluate the accuracy of the proposed approach, coupled stress-seepage analysis was performed for a period of 10 years before and 29 years after the construction of the tunnel. The mechanical and hydraulic behavior of the lining are described in terms of the displacement of the tunnel invert, the water flow rate through the RC lining, the pore water pressure, and the water head in the soil around the tunnel. In the case of availability of field data, the numerical results are supported by comparison with the measurement values.

### 6.1. Mechanical behavior

The proposed approach is used to obtain the long-term vertical displacement at the tunnel invert for each year. Fig. 15 shows the predicted amount of difference in the vertical displacement between 2001 and 2010 along with the field measurement. Negligible amounts of settlement beneath the embankment area and large values of settlement outside this area are detectable. The maximum values of the recorded field settlement and numerical prediction are 11.9 mm and 21.3 mm, respectively. The calculated results are roughly agreeable to the measured results. However, some locations along the tunnel are disagreeable. One of the reasons is that the proposed FEM model of ground soils is created based on the limited information of boring holes, and the linear change between boring holes are assumed. The other reason is that the uniform ring model without ring joints is used for segmental lining and elastic parameters are considered for segment concrete material, but actual rings are interconnected by steel bolts and the material is non-linear. The proposed model can predict the overall behavior in the longitudinal direction of the tunnel. It may be difficult to predict all the detailed behavior of the tunnel.

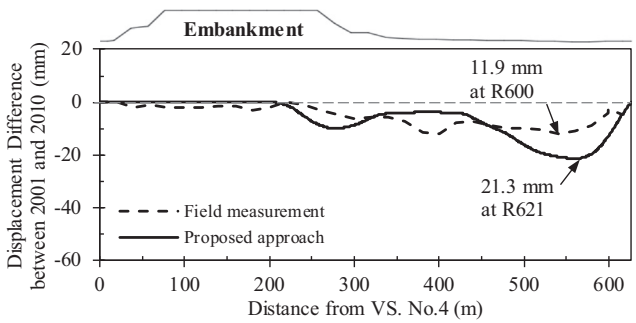


Fig. 15. Displacement difference between 2001 and 2010.

### 6.2. Hydraulic behavior

In this section, the hydraulic behavior of the lining is demonstrated in terms of the pore water pressure ($u$), water flow rate, and pressure water head for the soil around the tunnel.

Fig. 16 shows the changes in the predicted pore water pressure from 1971 to 2010 at R295 and R537, as well as a comparison with the annual average values of field measured data in Fig. 6 from 2008 to 2010. The calculated value of the initial hydrostatic pore water pressure at R295 and R537 are 153 kPa and 148 kPa, respectively (see Fig. 16).

R295 is under the edge of the embankment; the embankment load pore water pressure increased significantly to 187 kPa, and it then dissipated during nearly two years and reached the initial hydrostatic value. By excavation of the tunnel in 1981, a new drainage boundary to the surrounding clayey soils was introduced and the $u$ value reduced to 127 kPa as the lining permeability value ($k_t$) increased on the basis of the graph shown in Fig. 13. After 2002, the lining permeability was calculated by the deformed shape of the lining at each step. The numerical results show that for R295, $k_t$ of the lining approaches the value of the fully permeable lining. This can be checked by observing the predicted values ($k_t$) for R292 in Fig. 18, which is a few meters away from R295.

For R537, $k_t$ of the lining increased linearly before 2002 and the pore water pressure reduced smoothly from its

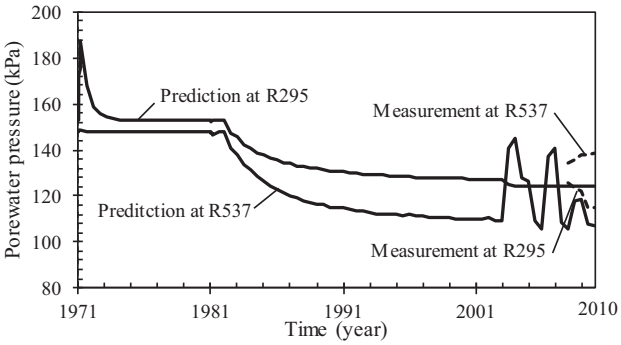


Fig. 16. Values of measured and predicted pore water pressure by time at R295 and R537.

Table 5
Widening and shrinkage condition of ring joint opening at R537.

| Year | R400 | | | R537 | | |
|---|---|---|---|---|---|---|
| | θ | Max. crown opening (μm) | Max. invert opening (μm) | θ | Max. crown opening (μm) | Max. invert opening (μm) |
| 2003 | 5.93E−06 | 0 | 23.70 | 1.84E−06 | 7.34 | 0 |
| 2004 | 6.18E−06 | 0 | 24.73 | 2.47E−07 | 0.99 | 0 |
| 2005 | 4.53E−06 | 0 | 18.13 | 1.38E−05 | 55.14 | 0 |
| 2006 | 2.89E−06 | 0 | 11.57 | 2.72E−06 | 10.88 | 0 |
| 2007 | 1.51E−06 | 0 | 6.05 | 1.58E−05 | 63.06 | 0 |
| 2008 | 4.01E−06 | 0 | 16.02 | 1.96E−06 | 0 | 7.85 |
| 2009 | 1.19E−05 | 0 | 47.58 | 7.01E−06 | 28.06 | 0 |
| 2010 | 6.22E−06 | 0 | 24.89 | 2.97E−06 | 11.89 | 0 |

hydrostatic value in 1981 to 109 kPa. After 2002, alternate increase and decrease in the pore water pressure occurred because of repetitive widening and shrinkage of the ring joint opening in the longitudinal direction of the tunnel. Table 5 summarizes the predicted changes in the joint opening for R537 at the tunnel invert and crown from 2002 to 2010. For instance, from 2003 to 2004, the crown opening shrank from 7.34 to 0.99 μm. By using Eqs. (2) and (3), the reduced lining permeability is introduced into the model, which leads to an increase in the value of the pore water pressure in the soil around R537. In the next year, the ring joint widens and the pore water pressure decreases. The actual annual changes in the pore water pressure in the field around the tunnels with deteriorated linings are thought to be zigzag in shape. The smooth changes in the predicted pore water pressure before 2002 owing to linear changes in $k_t$ as shown in Fig. 13 are believed to be close to the average values of the actual pore water pressure.

The porewater pressure at the section of R295 has different behaviors from R537. Because R295 is under the edge of the embankment, the ground soils experienced consolidation which was induced by embankment loading. The surrounding soils at R295 become much stiffer than the soils at R537, in this case, the soil resistance to the movement of tunnel linings at R295 is stronger than the one at R537. It can be considered that R537 moves easily due to changes in effective stress of surrounding clayey soils. According to Table 5, in almost all cases, the ring joint at R537 opened or closeed from the crown. The exception is 2008: this is because the proposed numerical analysis predicted longitudinal concave deformation around R537 in 2008, while it predicted the convex deformation in other years. The predicted opening at R537 is also related to the longitudinal deformation of the neighbour rings along the tunnel.

Fig. 17 shows the predicted variations of the water flow rate through the lining of four sections along the tunnel by time. The sections at R186 and R292 are beneath the embankment, and the sections at R400 and R643 are beyond the embankment area. According to Fig. 5, the leakage at R186 is extremely limited and $k_t$ at this section is kept constant. Further, $k_t$ at the other sections is calculated using Fig. 13 before 2002, and after that, it is determined on the basis of the deformed shape of the lining in the longitudinal direction. The water flow rate changes significantly at R400. It increases and decreases due to the ring joint opening predicted by the proposed method shown in Table 5. A large opening of the ring joint allows for a high water flow rate. However, the water flow rate at R292 and R643 remains constant with a large value due to the large deformation at the edge of the embankment and the end of the tunnel for the tunnel linings in the longitudinal direction (see Fig. 15). This can be attributed to the different stiffness of ground soils and boundary connection with the rigid structure of vertical shaft, respectively.

Fig. 18 shows predicted the relationship between the water flow rate and the lining permeability $k_t$ at sections

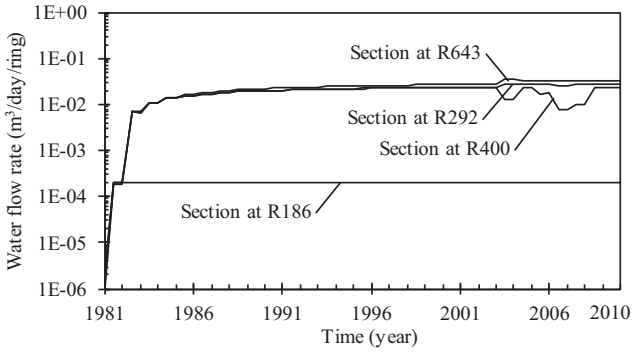


Fig. 17. Predicted values of water flow rate with time at R186, R292, R400, and R643.

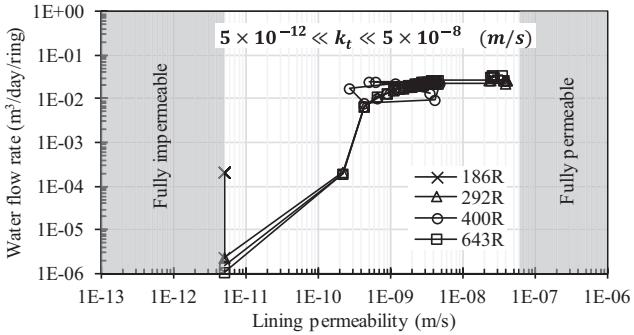


Fig. 18. Predicted relationship between water flow rate and lining permeability at R186, R292, R400, and R643.

R186, R292, R400, and R643. It can be seen that at R186, $k_t$ is equal to $5.0 \times 10^{-12}$ m/s and the water flow rate is limited to $2.1 \times 10^{-4}$ m$^3$/day/ring. At the other sections, the water flow rate increases with $k_t$ and reaches a maximum of $3.3 \times 10^{-2}$ m$^3$/day/ring as $k_t$ approaches $5.0 \times 10^{-9}$ m/s. When $k_t$ exceeds $5.0 \times 10^{-9}$ m/s, the water flow rate is nearly unchanged. It can be seen that the water flow rate by lining permeability in Fig. 18 has similar and conjoint behaviors in Fig. 17.

Fig. 19 shows changes in the pressure water head by time. The pressure water head at R186 and R292 increases by the effect of the embankment load and behaves similarly to that at R295 as shown in Fig. 16. The pressure water head at R186 remains unchanged, but for R292 and R643 sections, it reduces from the initial hydrostatic value to approximately 1.9 m in 2002. After 2002 it gradually decreases to nearly zero because the lining permeability $k_t$ is obtained by the opening of ring joints after that time. The ring joints opened relatively large at R292 and R643, and the two rings became fully permeable. This results in the pressure water head decrease to almost zero. However, the pressure water head at R400 increases and decreases significantly which is induced by the changes in lining permeability (see Fig. 18), and the lining permeability is predicted by the ring joint opening (see Table 5). There was no field measurement data of the water head.

## 7. Effect of temperature on lining behavior

Seasonal changes in temperature inside the tunnel result in the expansion and shrinkage of the concrete segment volume, which consequently alter the opening of the ring joints. The variation in the ring joint opening and temperature inside the tunnel shown in Fig. 8 indicate that the opening of the ring joints changed during one year and then nearly returned back to its initial value at the end of 2002. It is believed that this pattern of ring joint opening is repeated each year. This means that in 2002 and later (and probably even before that), the variation of the lining permeability is mainly because of seasonal changes in temperature inside the tunnel, and the effect of consolidation is extremely small. Therefore, it is important to evaluate the lining permeability by considering the temperature effect.

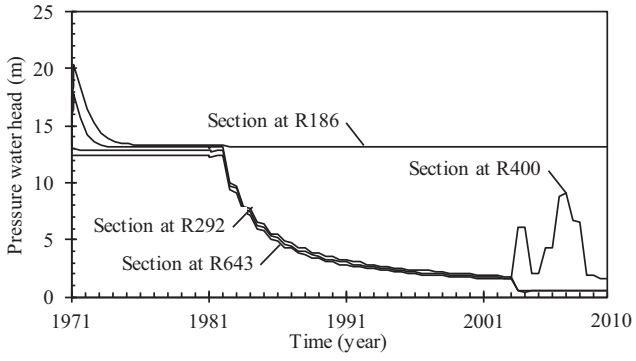


Fig. 19. Predicted values of pressure water head with time at R186, R292, R400, and R643.

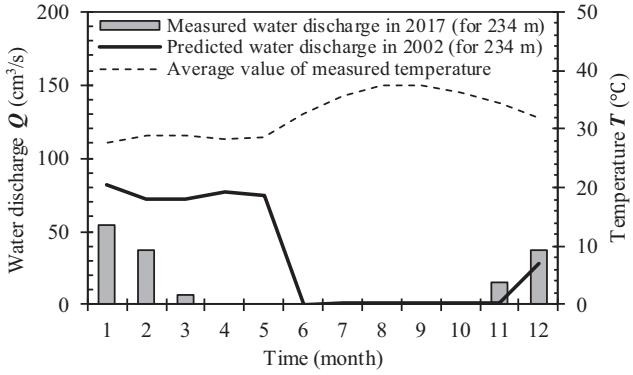


Fig. 20. Measured and predicted water discharge related to temperature change with time.

For the purpose of analyses in this part, $k_t$ before 2002 is determined using the changes in temperature inside the tunnel as shown in Fig. 8 and proposed by Eq. (6). By introducing $k_t$ into the model, the water discharge value in 2002 is calculated. Fig. 20 shows the predicted water discharge in 2002 for 234 m along the tunnel between VS No. 4 and VS No. 5. Water discharge in the field was also measured in 2017 for 234 m along the tunnel.

As discussed above, it is believed that the ring joint opening pattern is repeated every year and the consolidation effect is small after 2002; therefore, the measured value in 2017 could be compared with the predicted one in 2002.

Both the predicted and measured values of water discharge indicate nearly no discharge during the hot season and considerable leakage in the cold season. The overall behavior of the lining can be predicted using the numerical model; however, a small discrepancy between the two might exist because of the small effect of consolidation that has not been considered in 2002 by numerical analysis.

## 8. Conclusion

In this study, the long-term mechanical and hydraulic behavior of a segmented tunnel in soft clay was investigated by focusing on the lining permeability during the life of the tunnel. A method was proposed to determine the lining permeability based on the opening of joints between rings only. The proposed method was implemented in a coupled soil-water numerical model along with the long-term field data of an old tunnel in Japan to verify its accuracy.

It was also shown that in the final stages of the consolidation process, seasonal temperature changes inside the tunnel play an important role in the lining permeability. Using the measured data of the seasonal temperature changes inside the tunnel in this study, the lining perme-

ability was correlated with the seasonal temperature. The findings of this paper are as follows.

(1) Using the recommendations for permeability values in jointed rock, the lining permeability of a tunnel located in soft clay was related to the opening of joints between the rings. Depending on the location of the maximum opening (whether it is at the crown or at the invert), longitudinal deformation of the tunnel under long-term consolidation can be obtained. In addition, by variation of the joint opening, the lining permeability in the range of fully impermeable to fully permeable can be defined for any tunnel under similar conditions.
(2) A relationship between the lining permeability and the temperature change inside the tunnel was proposed in the final stages of consolidation when the pore pressure changes and water leakage nearly reached a steady-state condition. It was shown that under seasonal temperature changes inside the tunnel, widening and shrinkage of the ring joint opening were repeated annually by volumetric strain of the concrete segment volume. Therefore, in this state, the tunnel lining had a greater influence on the temperature effect than the consolidation effect. Using the proposed temperature-lining permeability correlation, the temperature-dependent consolidation of soil around the tunnel in soft clay was studied and pertinent water discharge values were compared with the measurement values. The overall behavior of the lining under the temperature effect was similar to the measured one.
(3) The results of deformation at the invert of the tunnel, pore water pressure changes, and water flow rate obtained using the proposed method for the lining permeability and their comparison with the corresponding field measured data showed acceptable capability of the proposed method for use in numerical analysis of similar soil-water coupling problems.

It should be noted that although the findings are based on only one case study, the proposed method may be applicable to any old tunnel in soft clay under similar conditions. Future investigation may facilitate development of the proposed method by considering some more factors, such as roughness of the ring joint opening, resistance effect of the sealing rubber, and radial effect of water flow. There is a need for additional field measurement data on the long-term behavior of segmented tunnels in soft clayey soil.

## Acknowledgments

The authors would like to acknowledge the Tokyo Electric Power Company (TEPCO) and the Tokyo Electric Power Services Company (TEPSCO) for supporting the field measurement data during the research.

## References

Ariizumi, T., Kaneko, S., Enzi, S., 2006. Investigation on long-term load of shield tunnel. Tunnel Undergr. 37 (11), 865–872.
Davis, S.N., 1969. Porosity and permeability of natural materials. Flow Through Porous Media, 54–89.
Gourvenec, S.M., Mair, R.J., Bolton, M.D., Soga, K., 2005. Ground conditions around an old tunnel in London Clay. Proc. Inst. Civil Eng.-Geotech. Eng., 158(1), 25–34.
Harris, D.I., 2002. Long term settlement following tunnelling in overconsolidated London Clay. Geotechnical aspects of underground construction in soft ground. Spécifique, Lyon, 393–398.
Huitt, J.L., 1956. Fluid flow in simulated fractures. AIChE J. 2 (2), 259–264.
Laver, R.G., Li, Z., Soga, K., 2016. Method to evaluate the long-term surface movements by tunneling in London clay. J. Geotech. Geoenviron. Eng. 143 (3), 06016023.
Li, Z., Soga, K., Wright, P., 2015. Long-term performance of cast-iron tunnel cross passage in London clay. Tunn. Undergr. Space Technol. 50, 152–170.
Louis, C., 1969. A study of groundwater flow in jointed rock and its influence on the stability of rock masses, Imperial College. Rock Mechanics Research Report 10, 1–90.
Maini, Y.N., 1972. In situ hydraulic parameters in jointed rock–Their measurement and interpretation.
Mair, R.J., 2008. Tunnelling and geotechnics: new horizons. Géotechnique 58 (9), 695–736.
Mair, R.J., Taylor, R.N. (1997, September). Bored tunnelling in the urban environment (State-of-the-art report and theme lecture). In: Proceedings of the 14th International Conference on Soil Mechanics and Foundation Engineering, AA Balkema, pp. 2353–2385.
Murillo, C.A., Shin, J.H., Kim, K.H., Colmenares, J.E., 2014. Performance tests of geotextile permeability for tunnel drainage systems. KSCE J. Civ. Eng. 18 (3), 827–830.
No, W. G., & International Tunnelling Association, 2000. Guidelines for the design of shield tunnel lining. Tunnelling and Underground Space Technology, 15(3), 303–331.
Oka, S., Ito, Y., Yokota, A., Saito, J., Kaneko, S., & Akagi, H., 2017. Long term prediction of vertical earth pressure loading on a shield tunnel in soft clay ground. Journal of Japan Society of Civil Engineers, Ser. F1 (Tunnel Engineering), 73(3).
Ports, D.M., Zdravkovic, L., 2001. Finite element analysis in Geotechnical engineering.
Sharp, J.C., 1970. Fluid flow through fissured media.
Nyren, R.J., 1998. Field measurements above twin tunnels in clay. Ph.D. thesis, Imperial Col. Sci. Tech. Med., London.
Shen, S.L., Wu, H.N., Cui, Y.J., Yin, Z.Y., 2014. Long-term settlement behaviour of metro tunnels in the soft deposits of Shanghai. Tunn. Undergr. Space Technol. 40, 309–323.
Shin, J.H., Kim, S.H., Shin, Y.S., 2012. Long-term mechanical and hydraulic interaction and leakage evaluation of segmented tunnels. Soils Found. 52 (1), 38–48.
Shirlaw, J.N., 1995. Observed and calculated pore pressures and deformations induced by an earth balance shield: discussion. Can. Geotech. J. 32 (1), 181–189.
Snow, D. T., 1968. Rock fracture spacings, openings, and porosities. Journal of Soil Mechanics & Foundations Div.
Soga, K., Laver, R.G., Li, Z., 2017. Long-term tunnel behaviour and ground movements after tunnelling in clayey soils. Underground Space 2 (3), 149–167.
Tunnel Library 23, 2010. Design of Segment for Shield Tunnel (Revised version). JSCE
Ward, W.H., 1981. Tunneling in soft ground-general report. In: Proceedings of the Tenth International Conference on Soil Mechanics and Foundation Engineering, 1981 (Vol. 4, pp. 261–275).
Wongsaroj, J., Soga, K., Mair, R.J., 2011. Modelling of long-term ground response to tunnelling under St James's. In: Park, London (Ed.), Stiff

Sedimentary Clays: Genesis and Engineering Behaviour: Géotechnique Symposium in Print 2007. Thomas Telford Ltd., pp. 253–268.
Wongsaroj, J., Soga, K., Mair, R.J., 2013. Tunnelling-induced consolidation settlements in London Clay. Géotechnique 63 (13), 1103.
Wu, H., Xu, Y., Shen, S.L., Chai, J.C., 2011. Long-term settlement behaviour of ground around shield tunnel due to leakage of water in soft deposit of Shanghai. Front. Archit. Civil Eng. China 5 (2), 194–198.
Wyllie, D.C., Mah, C., 2014. Rock Slope Engineering. CRC Press.
Zhang, D.M., Liu, Y., Huang, H.W., 2013. Leakage-induced settlement of ground and shield tunnel in soft clay. J. Tongji Univ. (natural science) 41 (8), 1185–1190.